Chapter: 5

Fabrication of gelatin coated polycaprolactone nanofiber scaffolds co-loaded with luliconazole and naringenin for the treatment of *Candida* infected diabetic wounds

5 Fabrication of gelatin coated polycaprolactone nanofiber scaffolds co-loaded with luliconazole and naringenin for treatment of *candida* infected diabetic wounds

5.1 Plan of study

1. **Fabrication of gelatin coated PCL nanofibers**
2. **Morphological characterization of dual drug loaded gelatin coated PCL nanofibers mat**
    a. Transmission electron microscopy
    b. Scanning electron microscopy
    c. Atomic force microscopy
3. **Solid state characterization**
    a. Fourier transformative infrared spectroscopy (FTIR)
    b. X-ray diffraction spectroscopy (XRD)
    c. Differential scanning calorimetry (DSC)
4. ***In-vitro* Characterization**
    a. Surface pH study
    b. Contact angle Study
    c. Water vapour transmission rate
    d. % Water uptake capacity
    e. Entrapment efficiency
    f. Content and weight uniformity
    g. *In-vitro* drug release
    h. Drug release kinetic modelling
    i. Antifungal and antibiofilm activity
    j. Cytocompatibility study
    k. Hemocompatibility study
5. ***In-vivo* Characterization**

a. Wound closure study

b. Histopathological examination

c. Laser doppler examination

5.2 Materials

Luliconazole (LTZ) was generously provided by Dr. Reddy's Laboratories, Hyderabad, India as gift sample. Naringenin (NAR) was procured form Carbanio, India. The Polycaprolactone (PCL) (inherent viscosity 1.23dL/g) was generously provided by Corbion, Netherlands. Gelatin (GL) of a high molecular weight were procured from HIMEDIA, India. All other solvent and chemicals were of analytical or biological grade and were procured from certified vendor.

5.3 Methods

5.3.1 Optimization of gelatin coated PCL nanofiber scaffolds

GL-coated PCL nanofibers were prepared using a biaxial needle as per the literature, with minor modifications using electrospinning method [273]. The drug and polymers were weighted as per the scheme described in Table 5.1. For the core solution, a 7% w/v polycaprolactone solution was prepared using a solvent cocktail of chloroform ($CHCl_3$) and dimethyl formamide (DMF) in a 7:3 ratio. Similarly, a 12% w/v gelatin solution was prepared in water, acetic acid, and ethyl acetate in a 4:4:2 ratio. Finally, both solutions were filled individually into the syringe and transferred into the electrospinning system. The flow rate was maintained at a ratio of 3:1 with a spinning voltage of 2.5 KV/cm.

Table 5.1 Schematic representation of polymer and solvent ratio for nanofiber preparation.

S.No.	Nanofiber Type	PCL (%w/v)	GL (%w/v)	NAR (%w/w)	LTZ (%w/w)	Solvent Ratio
1	PCL nanofiber (PCL)	12	-	5	5	$CHCl_3$: DMF (7:3)
2	GL-PCL nanofiber (GL-PCL)	7	12	-	-	PCL in $CHCl_3$:DMF (7:3) and gelatin in Water: acetic acid: ethyl acetate (4:4:2)
3	NAR loaded GL-PCL nanofiber (GL-PCL-NAR)	7	12	-	-	PCL in $CHCl_3$:DMF (7:3) and gelatin in Water: acetic acid: ethyl acetate (4:4:2)
4	LTZ loaded GL-PCL nanofiber (GL-PCL-LTZ)	7	12	-	5	PCL in $CHCl_3$:DMF (7:3) and gelatin in Water: acetic acid: ethyl acetate (4:4:2)
5	NAR and LTZ co-loaded GL-PCL nanofiber (GL-PCL-LTZ/NAR)	7	12	5	5	PCL in $CHCl_3$:DMF (7:3) and gelatin in Water: acetic acid: ethyl acetate (4:4:2)

5.3.2 Morphological characterization

The TEM analysis was conducted using an FEI transmission electron microscope and a 300-mesh carbon-coated copper grid for sample deposition as per the literature [273]. The spun nanofiber was deposited onto the copper grid by placing it close to the electrospinning collector. Subsequently, the prepared sample grid was dried and loaded into TEM using a single slit sample holder and analysed at different magnifications. Similarly, confocal microscopy of nanofiber was performed to check the loading of drugs into GL-PCL nanofiber core using coumarin-6 dye. The coumarin-6 was loaded into the central core of

the GL-PCL nanofiber, and subsequent samples were prepared by spinning nanofiber over glass slide and observed using a confocal microscope [274].

For scanning electron microscopy (SEM) and scanning probe microscopy (SPM), a piece of nanofiber was cut from a nanofiber mat and fixed over a glass slide [275]. For SEM analysis, a thin layer of gold (Au) coating was applied over the nanofiber and examined using a Carl Zeiss EVOTM SEM MA15/18 scanning electron microscope at different magnifications. Similarly, for AFM analysis, the prepared nanofiber sample was scanned using the NT-MDT NTEGRA Prima^{TM} instrument and analysed using NOVA™ software to characterize the 3D morphology of nanofibers.

5.3.3 Solid state characterization

To evaluate the crystallinity, thermal behaviour, compatibility and entrapment of drugs within the nanofiber matrix Fourier-transform infrared spectroscopy (FTIR), x-ray diffraction spectroscopy (XRD), and differential scanning calorimetry (DSC) study of drug, polymers and nanofibers were conducted. The Fourier transfor infrared (FTIR) spectroscopy was performed using literature [276]. Briefly, a series of drug, polymer, and nanofiber samples were placed on a sample stand, and transmission spectras were recorded within the spectral range of 4000 cm^{-1} to 400 cm^{-1}, employing a total of 60 scans using the Bruker Alpha^{TM} instrument.

For X-ray diffraction spectroscopy, drugs, polymers, and nanofibers samples were spread over an XRD sample holder and scanned using a 2Ɵ range of 5° to 65° using the Rigaku Miniflex instrument. Further, differential scanning calorimetry (DSC) analysis was conducted using a Shimadzu DSC-60 Plus instrument as per the literature [277]. The sample was placed in an aluminium crucible and sealed using a hydraulic press. Then, the sealed crucible was placed over the sample holder and analysed between 25°C and 350°C, with a heating rate of 10°C/min and a nitrogen flow rate of 40 mL/min.

5.3.4 Water contact angle & surface pH study

The water contact angle of the nanofiber membrane was determined using the Kruss™ DSA30E contact angle instrument as per the literature [278,279]. The nanofiber membrane was placed on the sample stand, and 20 µL of water droplets were dropped over its surface. The images of nanofiber and water droplets at the interface were captured using a CF04 camera and analysed to find the water contact angle.

Similarly, the surface pH of the nanofiber surface was determined by touching the probe of the pH meter to the wet nanofiber surface as per the literature [280]. A 2 mg nanofiber sample was cut from the nanofiber mat and transferred into a 5 mL petri plate. Then, the surface of the nanofiber was saturated with buffer, followed by pH measurement by touching the probe of the pH meter.

5.3.5 Water absorption capacity and vapour transmission rate

The water absorption capacity study was determined to check the capability of GL, PCL, GL-PCL, GL-PCL-LTZ, GL-PCL-NAR and GL-PCL-LTZ/NAR nanofibers to absorb wound exudate [224]. For this 10 mg of nanofiber pieces were collected from freshly prepared nanofiber mat and immersed into pH7.4 phosphate buffer saline for 12 hours. After 12 hours nanofiber aliquots were removed from the buffer solution and weighted to calculate water uptake capacity (Equation 5.1).

$$\%\, Water\ uptake = \frac{Nanofiber\ final\ weight\ -\ Nanofiber\ Initial\ weight}{Nanofiber\ Initial\ weight}$$

Equation 5.1

Similarly, the water vapour transmission rate (WVTR) of nanofibers were evaluated [225,226]. For this glass tubes of mouth area 1.86 cm^2 were taken and filled with PBS buffer. After than mouth of the tubes were sealed with nanofiber and incubated at 37ºC for

12 hours. After 12 hours, weight of the tube tubes were recorded and water vapour transmission rate were calculated using Equation 5.2.

$$WVT = \frac{Initial\ weight\ of\ tube - Final\ weight\ of\ tube}{Area\ of\ tube * Time\ duration}$$

Equation 5.2

5.3.6 Entrapment efficiency and drug content uniformity

To evaluate the total drug loading and uniformity of drug distribution within nanofiber mats, entrapment efficiency, and content uniformity were calculated as per the literature [222,281]. Five samples of ~2 mg each were carefully cut from five distinct regions of the nanofiber mats. Then, each nanofiber piece was dissolved in 1 mL of trifluoroethanol to solubilize the drug and polymer completely. After solubilisation, this solution was added to 5 mL of methanol to precipitate out the polymers. Further centrifugation was carried out at 10,000 RPM for 6 minutes to precipitate the polymer ultimately. Finally, the supernatant obtained from the mixture was subjected to analysis using HPLC at a specific wavelength of 293 nm using a solvent system containing methanol and 0.1% v/v aq. orthophosphoric acid at a ratio of 70:30 with a flow rate of 1 mL/min.

5.3.7 Drug release profile

The drug release profiles of LTZ and NAR from the GL-PCL-NAR/LTZ nanofibers were investigated as described in the literature using the SpectraPro^{TM} MWCO > 1 kD membrane in PBS 7.4 pH buffer [236]. The 10 mg nanofiber membrane was cut from the nanofiber mats and placed in the dialysis membrane containing 2 mL of PBS 7.4 pH buffer. Then, the dialysis membrane was sealed from both ends and transferred into a 20 mL beaker containing 15 mL of 7.4 pH phosphate-buffered saline (PBS) solution. At regular intervals, a 0.5-mL sample was collected from the beaker and subjected to quantitative analysis using high-performance liquid chromatography (HPLC). Additionally, 0.5 mL of fresh media is

added to the outer compartment after every sampling to maintain sink condition. The findings of the examined samples have been correlated with various drug release models to forecast the drug release mechanism of drugs from nanofibers.

5.3.8 *In-vivo* release analysis

To visualize the release of drug from the GL-PCL-NAR/LTZ nanofibers, the DiD (1,1'-Dioctadecyl-3,3,3',3'-tetramethylindodicarbocyanine) dye-loaded nanofiber (4 µg/mL) was prepared as per the protocol described earlier [239,282]. The Sprague dawley rats, aged 12–14 weeks, were anesthetized and shaved to ensure the complete removal of hair. A full-thickness wound of ~1.5 cm^2 was then created on the dorsal region. Subsequently, the prepared nanofiber was applied to the wound site and monitored using an *in-vivo* imaging system (PhotonImager, Optima Biospace). The fluorescent signal was recorded at regular intervals for 60 hr and analysed using M3 Vision software (Bio Space Lab).

5.3.9 Antifungal and antibiofilm activity

The GL-PCL, GL-PCL-LTZ and GL-PCL-LTZ/NAR antifungal activity were determined by agar plate method against *C.albicans (ATCC 90028)*, *C.auris* (CDC-B11903), *and C.tropicalis* (ATCC 750), *C.parapsilosis (ATCC 22019)*, *C. krusei (ATCC 6258)* using CLSI guidelines and literature with minor modifications [283]. Briefly, 0.5 mL of microbial suspension ($1.5*10^8$ cells/mL) of each *Candida* species were prepared in normal saline and spread to Mueller-Hinton agar plates using cotton swabs. The petri plates were subsequently punched using a metal punch, and nanofiber aliquots weighing 2 mg were placed in their location. Then, each petri dish was placed in an incubator to maintain a temperature of 37 °C for 24 hr. After 24-hour incubation period, the zone of inhibition on each petri plate was quantified using a vernier caliper, and a high-resolution image was captured using a DSLR camera. The antibiofilm activity of GL-PCL and GL-PCL-LTZ/NAR was calculated over 48 hr, as per the protocol described in a previous study

[229]. Briefly, 15 mg of each nanofiber aliquot was transferred into the individual wells of a 32-well microplate and subsequently inoculated with 0.5 McFarland (~10^8 CFU/ml) of the corresponding fungal species for the incubation period of 48 hr. After 48 hr of incubation period, SEM analysis and MTT assays were performed to assess the percentage viability [230]. Similarly, the colony-forming ability of nanofibers was evaluated as per the protocol described with minor modifications[284,285]. Briefly, 5mg pieces of GL-PCL, GL-PCL-LTZ, and GL-PCL-LTZ/Nar nanofiber were treated in a previously prepared broth of respective fungi containing (CFU 10^6cells/mL). After 24 hours, the samples were diluted in PBS and spread over fresh plates to find the number of colonies in each group.

5.3.10 Hemocompatibility study

The hemocompatibility of GL-PCL, GL-PCL-LTZ, GL-PCL-NAR, GL-PCL-LTZ/NAR nanofibers were determined as per the reported work [184,231]. Briefly, 2 mg of nanofiber pieces were collected from nanofiber mats and incubated into diluted blood (2mL fresh blood + 3mL PBS 7.4 pH) for 60 min. After incubation, the nanofiber samples were centrifuged and percentage haemolysis were calculated (Equation 5.3) by taking supernatant absorbance at 545 nm.

$$\%\, Hemolysis = \frac{Test\ absorbance - Negative\ control\ absorbance}{Positive\ control\ absorbace - Negative\ control\ absorbance} * 100$$

Equation 5.3

5.3.11 *In-vitro* cytocompatibility study

The *in-vitro* cytocompatibility study of the GL-PCL and GL-PCL-LTZ/NAR nanofibers was done according to the protocol described in the literature, with a few modifications [232]. The human keratinocyte cells (HaCaT) were cultured in Dulbecco's Modified Eagle Medium (DMEM) supplemented with 10% fetal bovine serum (FBS) and Penistrep™

antibiotic solution in a CO_2 incubator at 37 °C and 5% CO2 concentration. To assess the cytocompatibility activity of GL-PCL and GL-PCL-LTZ/NAR nanofiber samples, pieces weighing 500 µg of each nanofiber were taken from a freshly prepared nanofiber mat (predried using vacuum desiccator for 24 hr) and placed in individual wells of a 6-well cell culture plate before cell seeding. The cell suspension, with a concentration of $3x10^4$ cells/mL, was evenly distributed into individual wells across three separate plates. For MTT assay (cell viability assay), the culture medium was aspirated and replaced with 300 µL of fresh medium containing MTT at 24, 48, and 72 hr post-incubation. The cells were then incubated for 2 hr at 37 °C. Following incubation, the formed formazan crystals were dissolved by adding 300 µL of dimethyl sulfoxide (DMSO). The solution was transferred into a 96-well cell culture plate to measure absorbance. The absorbance measurements were conducted at a wavelength of 570 nm. Also, following the incubation of nanofiber with cells, the images were acquired at various time intervals (24 hr, 48 hr, and 72 hr) using a phase contrast microscope equipped with an EVOS FL imaging system.

5.3.12 *In-vivo* wound healing activity

The wound healing activity of GL-PCL, GL-PCL-LTZ, GL-PCL-NAR, GL-PCL-LTZ/NAR nanofibers were evaluated against *C. albican* infected full-thickness wounds using 200–250 g of Sprague-Dawley (S.D) rats as per the IAEC application number **IIT(BHU)/IAEC/2023/II/005** and literature [286]. Diabetes was induced in S.D rats using streptozotocin and nicotinamide, as previously described in the publication [234,235]. In brief, rats were given 55 mg/kg streptozotocin and 120 mg/kg nicotinamide, with the nicotinamide given 15 minutes before the streptozotocin. After seven days of fasting, blood glucose levels were measured in all animals, and animals with blood glucose levels greater than 250 mg/dL were chosen for further research. The selected animals were divided into five distinct groups: GL-PCL, GL-PCL-NAR, GL-PCL-LTZ, and GL-PCL-LTZ/NAR

nanofiber, respectively, with each group containing three animals. Then, the dorsal region of each animal was carefully trimmed, followed by depilatory cream to eliminate any remaining hair and achieve a state of hairlessness on the skin surface. After that, a precise1.5cm diameter full-thickness wound was made over the dorsal part. A fresh *Candida* fungus suspension was made in normal saline and inoculated over the wound to mimic the infection. All animals with wounds were kept in a highly humid environment to further enhance the fungus infection for 4 days. After fungal infections, each group received respective treatments. Post treatment wounds condition of each groups animal were monitored regularly, images of wound were captured and granulated tissues were collected from wounds at day 12^{th} and 21^{st}

5.3.13 Histopathological study

The histopathological investigation of the wound tissue was performed to get insights about cellular and tissue-level changes within the wound site during the wound healing process, as per the protocol described in [236]. Briefly, the granulated tissue collected during the study were washed with phosphate-buffered saline (PBS) to remove any debris or contaminants and further stored in a formalin solution of 10% w/v. For the histological study, a tissue sample was fixed in a wax mould and a precise transverse section of 10-20µm thickness was cut using a microtome. The cut piece was fixed onto a glass slide and subjected to staining using the H&E staining. Finally, the stained slides were carefully examined under a Dewinter optical microscope using a 10X objective lens, and images were captured using Dewinter Bio Wizard software for further analysis.

5.3.14 Laser doppler study

The laser Doppler study assessed the blood flow across the wound surface [237]. Briefly, rats were anesthetized with ketamine and xylazine, and blood flow assessment was done

by placing the wound site under the path of a laser Doppler camera and analysed using OSMOZONE™ software.

5.3.15 Statistical analysis

All study results were statistically analysed using GraphPad Prism version 5.03. The results have a Mean$^{\#}$ ± standard deviation (S.D) ($^{\#}$n = 3). For group comparison, ANOVA and the student's t-test were used at statistical significance of *p < 0.05, **p < 0.01, ***p < 0.001, and ****p< 0.0001.

5.4 Results

5.4.1 Morphological characterization

The TEM analysis of GL-PCL shows the presence of a gelatin coating on the surface of the nanofibers (Figure 5.1A). The confocal microscope, revealed the presence of fluorescein intensity emanating from the nanofiber, as well as a visually distinct dark-coloured gelatin coating (Figure 5.2B). The SEM results of prepared PCL nanofiber showed a uniform distribution of nanofibers with an average diameter (Table 5.2) of 164.21±24.91 nm and a median diameter of 159.06 nm. These results match the earlier work reported in the publication [287,288]. The GL-PCL nanofibers results shows an average diameter of 213.35±52.55 nm and randomly aligned nanofibers morphology (Figure 1C). The GL-PCL-NAR and GL-PCL-LTZ nanofibers exhibit mean diameters of 341.48±115.56 nm and 354.99±97.33 nm, respectively. The fabricated nanofibers exhibit a size distribution ranging from small to medium-sized nanofibers. Further, the GL-PCL-LTZ/NAR nanofiber SEM results shows, interconnected but arranged nanofiber with a median diameter of 356.11 nm and average diameter of 379.67±166.62 nm (Figure 5.1D).

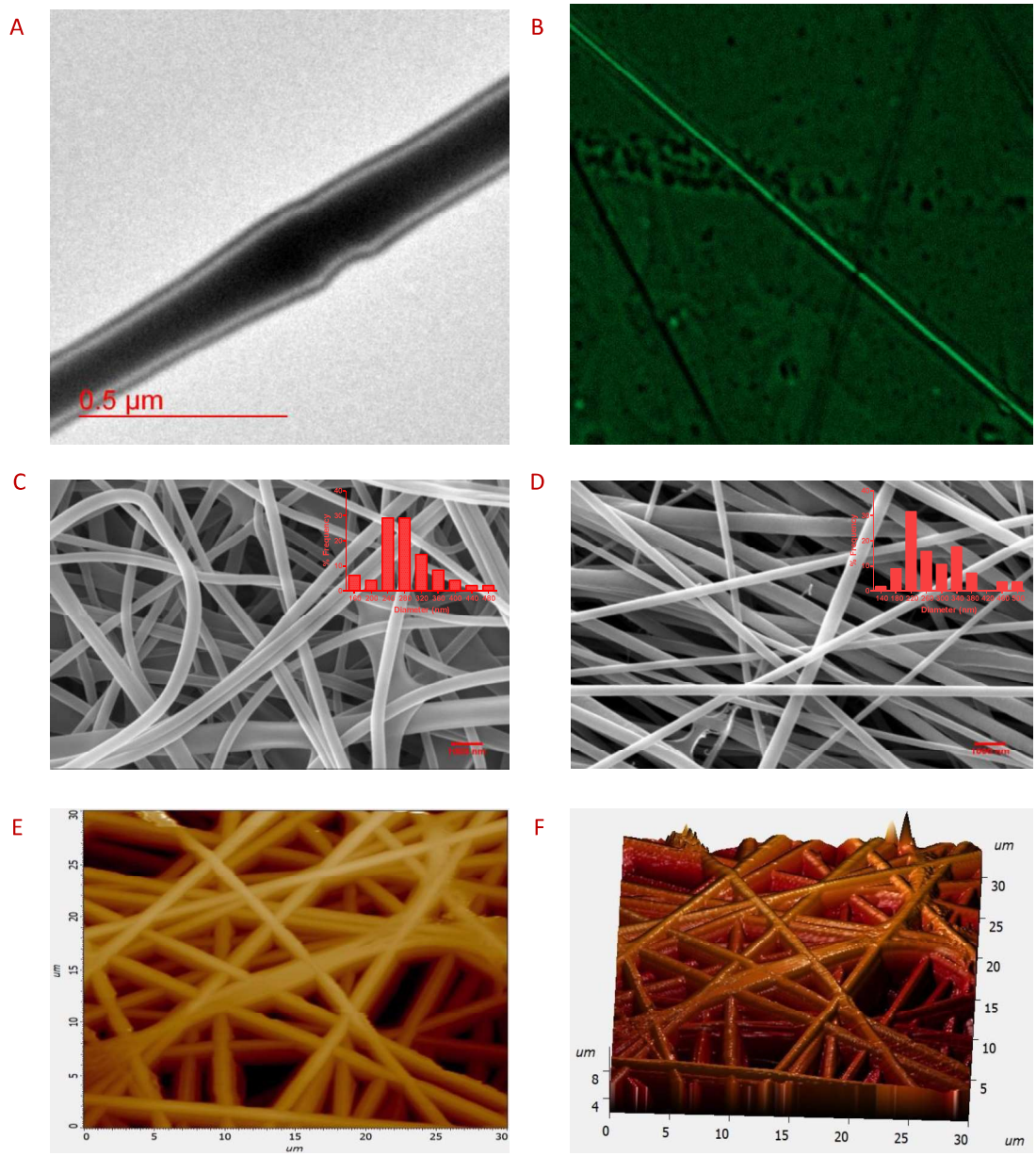

Figure 5.1 (A) Transmission electron image of prepared nanofiber; (B) Confocal Image of GL-PCL-Coumarin-6 loaded nanofiber; Scanning electron Image of GL-PCL (C) & GL-PCL-LTZ/NAR respectively (D); (E&F) 2D &3D AFM image of GL-PCL-LTZ/NAR.

The 2D and 3D AFM result of GL-PCL-NAR/LTZ showed nanofibers morphology similar to SEM (Figure 5.1 E&F) with average roughness and root mean square value of 0.531±0.12 µm and 0.746±0.25 µm, respectively. These values were higher in case of PCL nanofibers, which has average roughness and root mean square values of 1.495±0.38 µm and 1.669±0.49 µm, respectively, indicating that GL-PCL-LTZ/NAR nanofibers have smoother morphology than PCL nanofibers.

Table 5.2 Tabular representation of median diameter and average diameter of prepared nanofiber mats.

S.No.	Formulation	Median Diameter (nm)	Diameter (nm*)
1	PCL	159.06	164.21±24.91
2	GL-PCL	212.88	213.35±52.55
3	GL-PCL-NAR	313.01	341.48±115.56
4	GL-PCL-LTZ	343.54	354.99±97.33
5	GL-PCL-LTZ/NAR	356.11	379.67±166.62

***Represent Mean±S.D (n=150)**

5.4.2 Solid state characterization

5.4.3 FTIR Study

The FTIR spectra (Figure 5.2) of LTZ exhibit distinct peaks, include 796.19 cm^{-1}, which corresponds to the –C-Cl (stretching), 1578 cm^{-1} for the >C=C< aromatic group, 2196 cm^{-1} for the stretching of –CN, and 3032 cm^{-1} for the C-H alkene group similar to the literature [288,289]. The NAR exhibits characteristic peaks at 1600 $cm^{-1}$and 1515 cm^{-1} for C=O stretching, which match the literature findings [290,291]. PCL displays peaks at 2949 cm^{-1} for asymmetric CH_2 stretching, 2868 cm^{-1} for symmetric CH_2 stretching, 1723 cm^{-1} for carbonyl stretching, and 1290 cm^{-1} for C-C stretching [292].

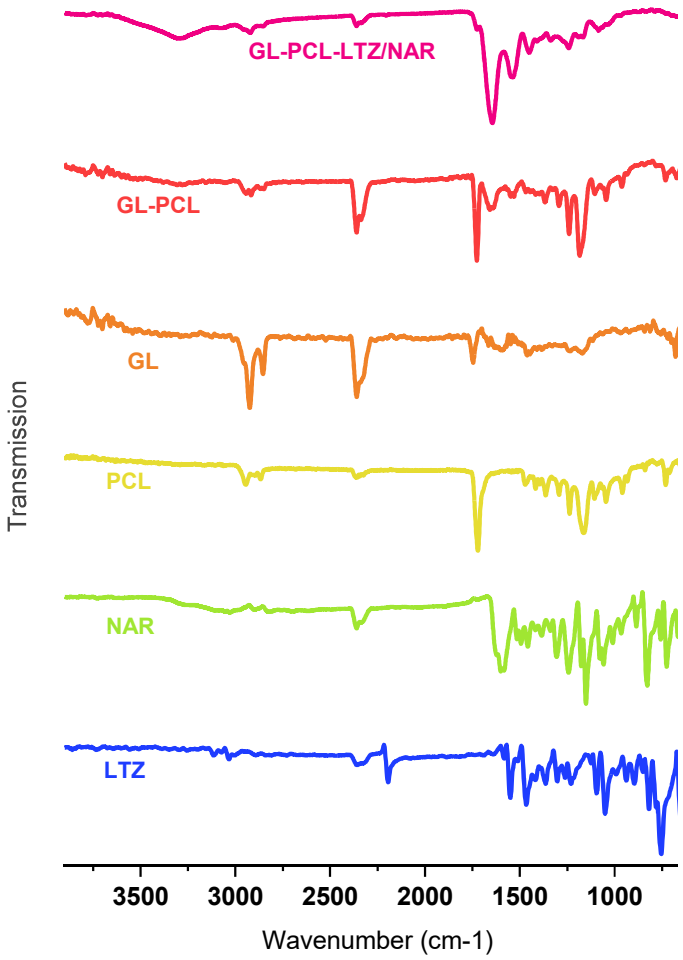

Figure 5.2 FTIR spectra of drugs (luliconazole and naringenin), polymer and prepared nanofibers with luliconazole (LTZ), naringenin (NAR), polycaprolactone (PCL), gelatin (GL), gelatin coated PCL nanofiber (GL-PCL), LTZ & NAR loaded gelatin coated PCL nanofiber (GL-PCL-LTZ/NAR).

The gelatin exhibits peaks at 1651 cm^{-1} and 1548 cm^{-1} for Amide I and Amide II, which match the literature [293]. The GL-PCL nanofiber spectra show peaks around 1650-1700 cm-1, which is around the gelatin region, and another peak for PCL. The GL-PCL-LTZ/NAR nanofiber shows sharp peaks of gelatin and some peaks of drugs and polymer.

5.4.3.1 X-ray diffraction Study

The X-ray diffraction (XRD) spectra (Figure 5.3) of LTZ exhibit sharp crystalline peaks at 13.66º, 16.36º, 18.38º, 21.18º, 23.32º, 24.48º, and 25.72º, as reported in the literature [294].

Conversely, NAR displays sharp crystalline peaks at 10.68°, 15.68°, 17.18°, 20.32°, 22.26°, and 23.72° [291,295].

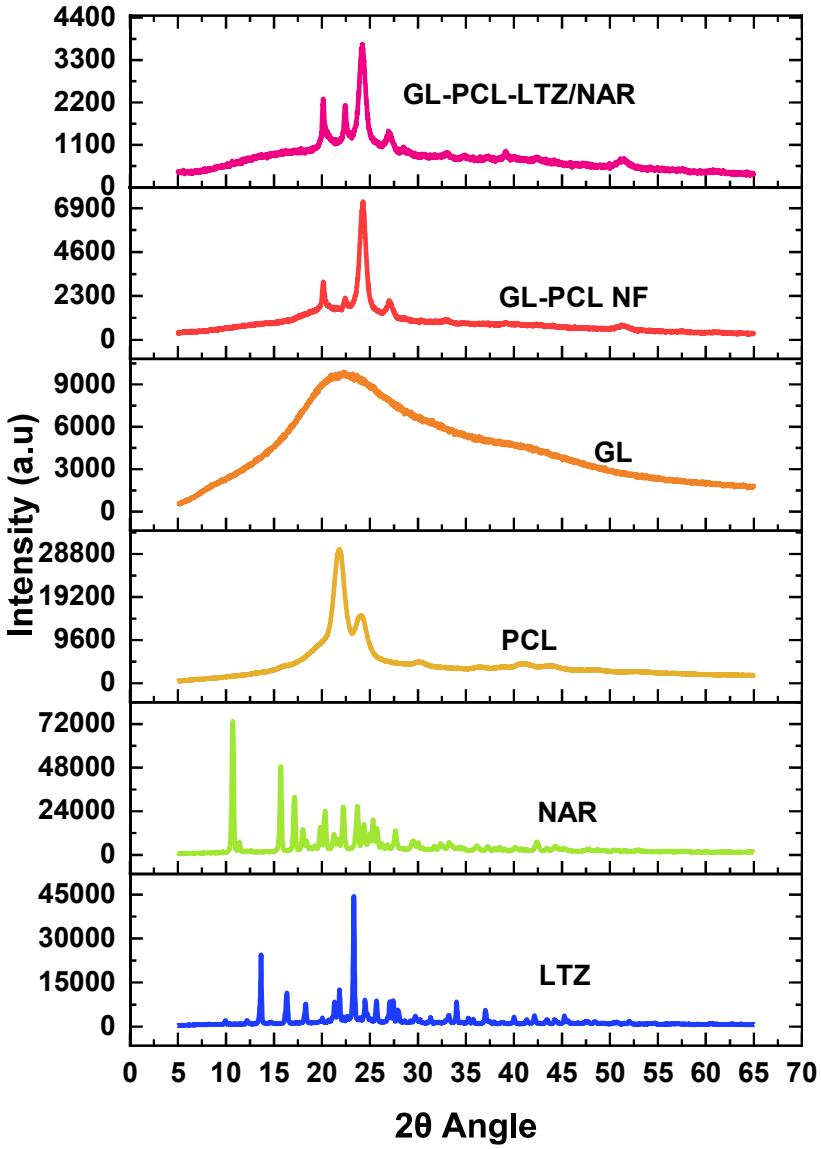

Figure 5.3 XRD spectra of drugs, polymer and prepared nanofibers with luliconazole (LTZ), naringenin (NAR), polycaprolactone (PCL), gelatin (GL), gelatin coated PCL nanofiber (GL-PCL), and LTZ & NAR loaded gelatin coated PCL nanofiber (GL-PCL-LTZ/NAR).

The PCL exhibits semi-crystalline peaks at 21.82° and 24.18° [295,296]. The gelatin exhibits an amorphous nature with a display of broad peaks. The GL-PCL-LTZ/NAR sample exhibits no peaks corresponding to nanofibers, indicating that the drug has been successfully entrapped within the polymeric matrix.

5.4.3.2 Differential scanning calorimetry study

The differential scanning calorimetry (DSC) thermogram (Figure 5.4) of LTZ and NAR exhibit distinct peaks at 152.47ºC and 254.93ºC, respectively. These peaks indicate the melting points of the drugs and align with previously reported findings in the literature [295,296]. PCL exhibits peaks at 64.87ºC, while gelatin, on the other hand, does not display distinct peaks, possibly owing to its amorphous characteristics [248]. The GL-PCL-LTZ/NAR spectra showed melting peaks of PCL and the absence of sharp drug melting peaks, which might be due to the uniform distribution of drugs in the nanofiber matrix.

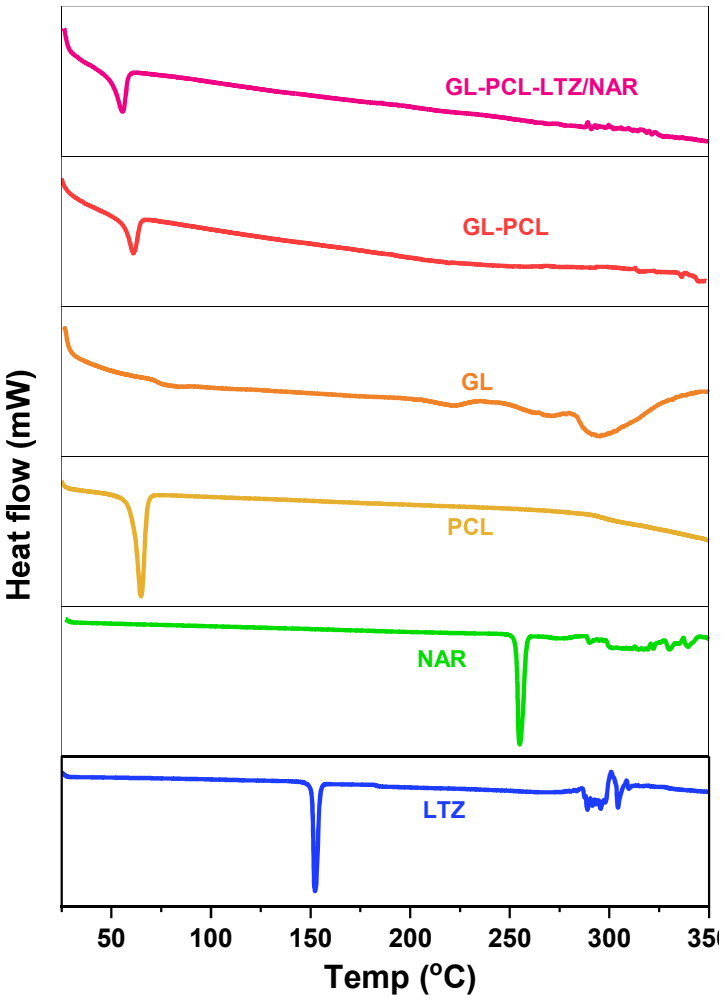

Figure 5.4 Differential scanning calorimetry thermogram of drugs, polymer, and formulation with luliconazole (LTZ), naringenin (NAR), polycaprolactone (PCL), gelatin (GL), gelatin coated PCL nanofiber (GL-PCL), LTZ & NAR loaded gelatin coated PCL nanofiber (GL-PCL-LTZ/NAR).

5.4.4 Water contact angle and surface pH study

The water contact angle of the PCL nanofiber, GL nanofiber, GL-PCL nanofiber, and GL-PCL-LTZ/NAR nanofiber is depicted in Figure No 5.5. The water contact angle of PCL nanofiber experienced a significant decrease from 84.5° to 26.6° after gelatin coating over the PCL nanofiber (Figure 5.5 A-C). Furthermore, the contact angle of GL-PCL-LTZ/NAR nanofiber showed a slight increase trend (Figure 5.5D), which could be attributed to the hydrophobic nature of NAR and LTZ [297]. Further, the surface pH (Figure 5.5 F) of the nanofibers was found to be in the range of 5.5-6.5, indicating their potential suitability for topical application [298].

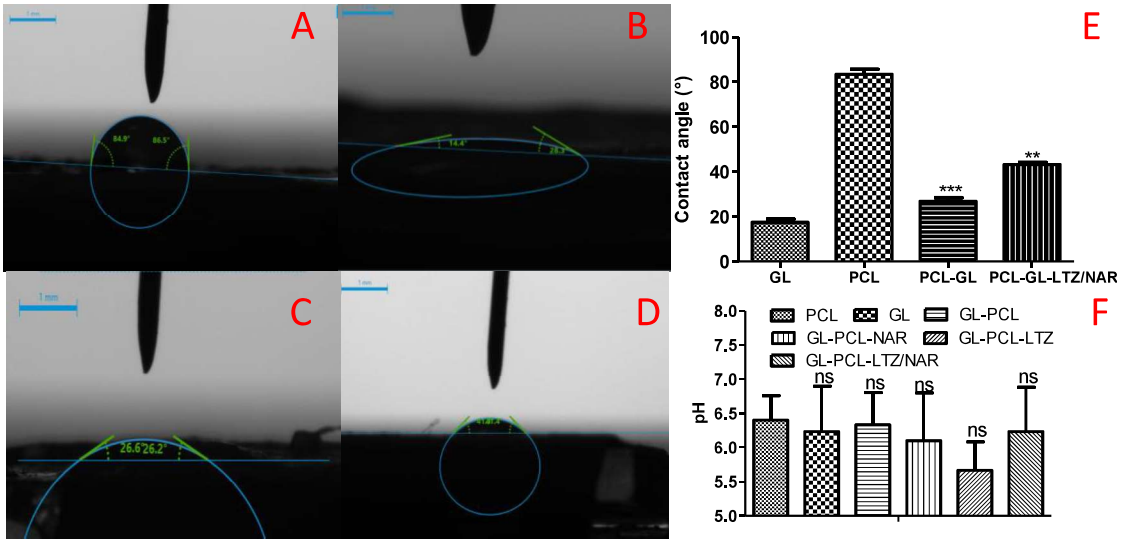

Figure 5.5 Contact angle image of (A) PCL nanofiber, (B) GL nanofiber, (C) GL-PCL Nanofiber, (D) GL-PCL-LTZ/NAR nanofiber; (E) Contact angle of different formulations; (F) Surface pH graph of different formulations (In all graphs vertical bars represent standard deviations (n=3), 'ns' represent non significant, ** represent p value < 0.01 and *** represent p value < 0.001).

5.4.5 Water absorption capacity and water vapour transmission rate (WVT)

The PCLNF showed water uptake of 56±6.9% as compared to the gelatin nanofiber which showed the water uptake 289±42%. The poor behaviour might be due to the hydrophobic nature of polycaprolactone. Further, the gelatin coated polycaprolactone nanofiber demonstrated the water uptake capacity of 169±12.6%, 156±18.9%, 160±21.3% and

149.3± 19.6%, respectively This significant (p value < 0.01) increase in the water uptake capacity (Figure 5.6A) of GL-PCL, GL-PCL-LTZ, GL-PCL-NAR and GL-PCL-LTZ/NAR nanofiber proves the effectiveness of gelatin coating over the surface of polycaprolactone nanofiber.

The GL-PCL, GL-PCL-LTZ, GL-PCL-NAR and GL-PCL-LTZ/NAR nanofiber showed the water vapour transmission rate in the range of 18-22 mg/cm^2/hr (Figure 5.6B). as compared to the open tube which have the water vapour transmission of 35±1.9 mg/cm^2/hr. This significant decrease in the vapour transmission (p value <0.05) would help in reducing the wound drying with maintaining gaseous exchange

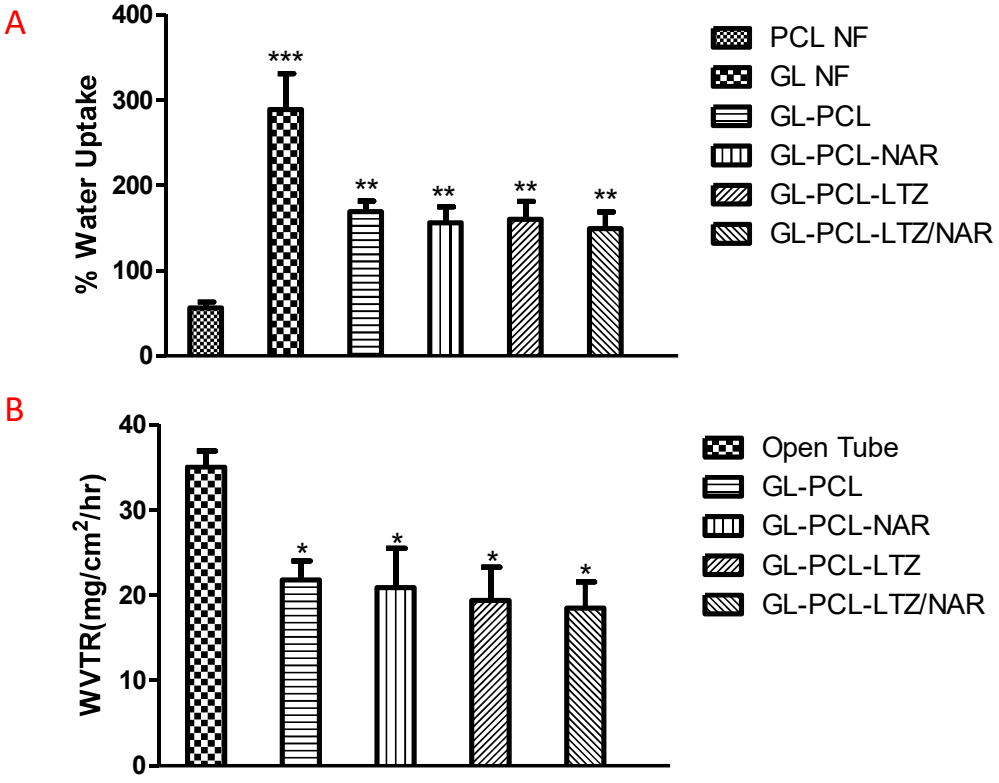

Figure 5.6 (A) % Water uptake capacity, (B) Water vapour transmission rate (WVTR) of different nanofibers (In both graph vertical bars represent standard deviation (n=3), * represent p value <0.05, and ** represent p value <0.01 and *** represent p value < 0.001).

5.4.6 Entrapment efficiency and drug content uniformity

The drug content uniformity and entrapment efficiency (EE) for different nanofiber formulations are shown in **Table 5.3**. The results show that PCL nanofiber shows an entrapment efficiency of 75.3±3.9% and 80.2±1.8% for LTZ and NAR, respectively. Similarly, the entrapment efficiency of LTZ in GL-PCL-LTZ was found to be 89.6±3.8%, while the entrapment efficiency of NAR in GL-PCL-NAR nanofiber was found to be 94.65±3.1%. The simultaneous loading of LTZ and NAR into GL-PCL nanofiber shows an entrapment efficiency of 85.1±3.4% for LTZ and 92.4±4.9% for NAR. The observed rise in entrapment efficiency could be due to increased nanofibers diameter in GL-PCL-LTZ/NAR. Further, the drug content uniformity result shows a standard deviation of less than 5%, which suggests a uniform demonstration of drugs in the nanofiber matrix.

Table 5.3 Entrapment efficiency of luliconazole and naringenin by different nanofibers

S.No.	Formulation	Luliconazole (% EE)*	Naringenin (% EE)*
1	PCL	75.3±3.9%	80.2±1.8%
2	GL-PCL	-	-
3	GL-PCL-NAR	-	94.65±3.1%
4	GL-PCL-LTZ	89.6±3.8%	-
5	GL-PCL-LTZ/NAR	85.1±3.4%	92.4±4.9%

*Data represent here as mean ± Standard deviation (n=3)

5.4.7 Drug release study

GL-PCL-LTZ/NAR nanofiber provided the release of LTZ and NAR for ~10 days, with cumulative percentage release of 93.58±2.93% for NAR and 67.8±3.21% for LTZ in 220 hr. (Figure 5.8A). During, initial phase of study GL-PCL-LTZ/NAR provided sharp release of NAR and LTZ with cumulative percentage releases of 23.2±3.43% and 12.1±2.6%, respectively in 1.5 hr. In later phase the drug release from the nanofiber was uniform up to

220 hr. The higher release of NAR in initial phase might be attributed due to its high aqueous solubility of NAR as compared to the LTZ. Furthermore, it's worth mentioning that initial sharp release of the drugs would be beneficial and facilitates faster minimum effective concentration at wound site. Additionally, kinetic modelling using zero order, first order, Higuchi, Korsemeyer-Peppas, Hixson Crowell, and Peppa's & Sahlin models (Figure 5.7) showed that the GL-PCL-LTZ/NAR formulation exhibits the highest coefficient of regression (r^2) values of 0.9980 and 0.9963 for NAR and LTZ, respectively, when employing the Peppas and Sahlin mathematical models. Furthermore, the obtained n value was found to be less than 0.45, indicating that the drug release from the nanofiber follows the fickian diffusion mechanism, which is related to the polymeric chain relaxation observed in gelatin and the polymer erosion observed in polycaprolactone [299].

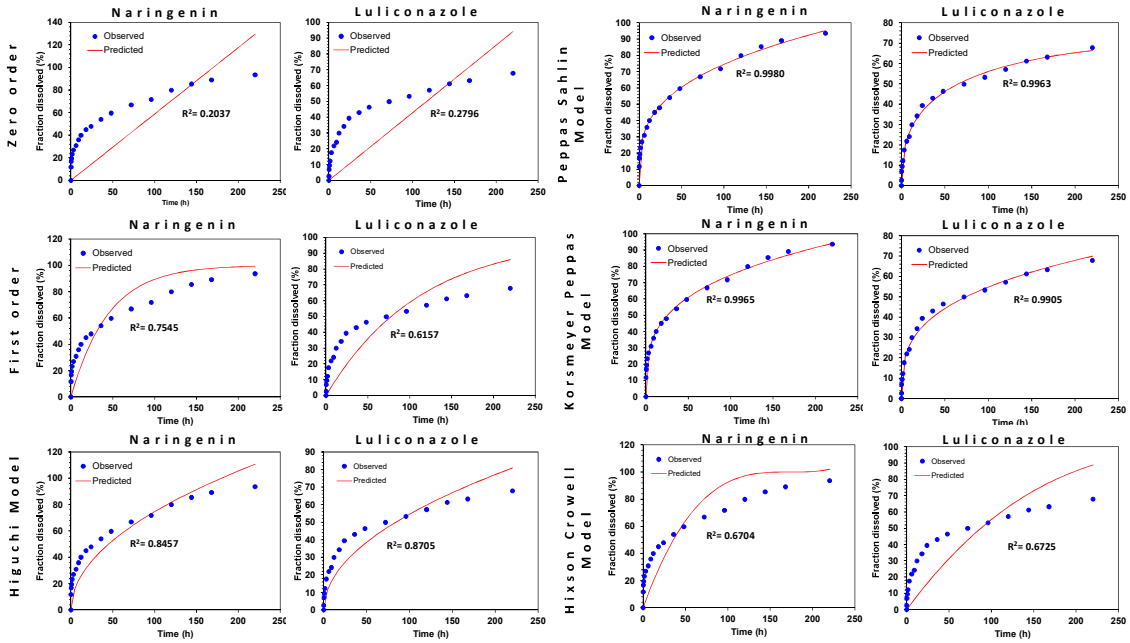

Figure 5.7 Drug release kinetic modelling of luliconazole and naringenin from GL/PCL-LTZ-NAR NF formulation

5.4.8 *In-vivo* imaging study

In-vivo imaging study showed fluorescent signals emitted by the DiD dye-loaded GL-PCL nanofiber around the wound area (Figure 5.8 C). The GL-PCL nanofiber initially provided

the sharp release of DiD dye with a maximum fluorescent count of $6.2x10^6$ at 12 hr (Figure 5.8 B). The initial intense release might be due to the swelling of the outer layer gelatin layer, which subsequently enhanced the migration of the drug. The release pattern was comparable to in-*vitro* drug release profile (Figure 5.8A) observed for the GL-PCL-LTZ/NAR nanofiber.

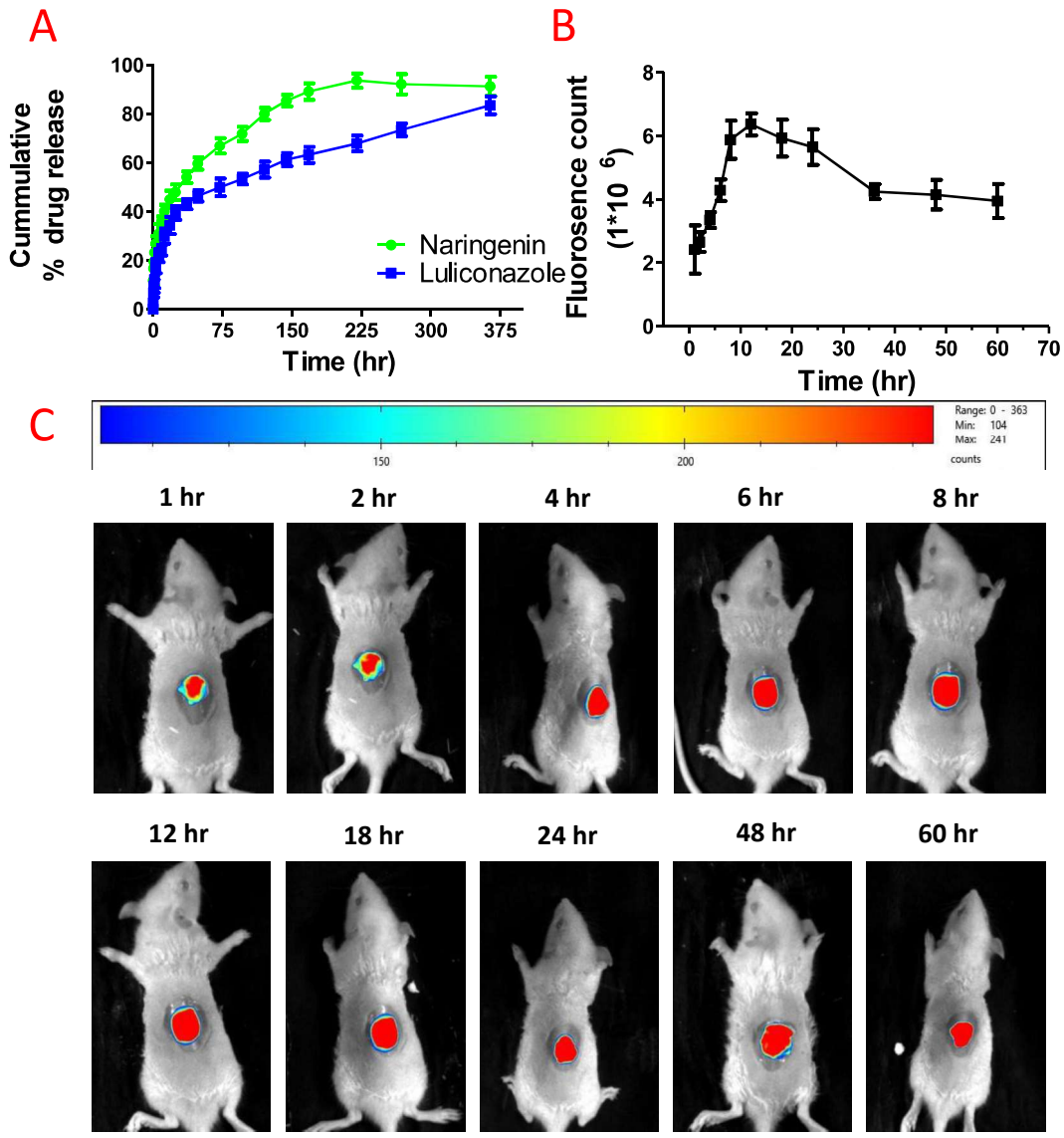

Figure 5.8 (A) Drug release profile of LTZ & NAR from GL-PCL-LTZ/NAR; (B) Fluorescence count vs Time graph of *In-vivo* release study (C) *In-vivo* release of DiD dye from GL-PCL nanofiber (vertical bars in all graphs represent standard deviations (n=3)).

5.4.9 Antifungal and antibiofilm activity

The GL-PCL-LTZ/NAR and GL-PCL-LTZ nanofiber groups demonstrated good antifungal activity against various *Candida* species (Figure 5.9 A-F). The study had shown the zones of inhibition of 36.350±0.86 mm and 39.207±2.86 mm against *C. albicans*, 30.86±1.2 mm and 21.20±1.22 mm against *C. auris*, 19.69±0.8 mm and 15.66±1.45 mm against *C. parapsilosis*, 28.205±3.35 mm and 24.160±2.30 mm against *C. tropicalis*, and 34.8±0.7 mm and 30.2±0.9 mm against *C. krusei*, for GL-PCL-LTZ/NAR and GL-PCL-LTZ, respectively. The blank nanofibers had not shown any discernible zone of inhibition. Similar, findings were observed in colony forming assay and lowest fungi colony was observed in GL-PCL-LTZ/NAR nanofiber.

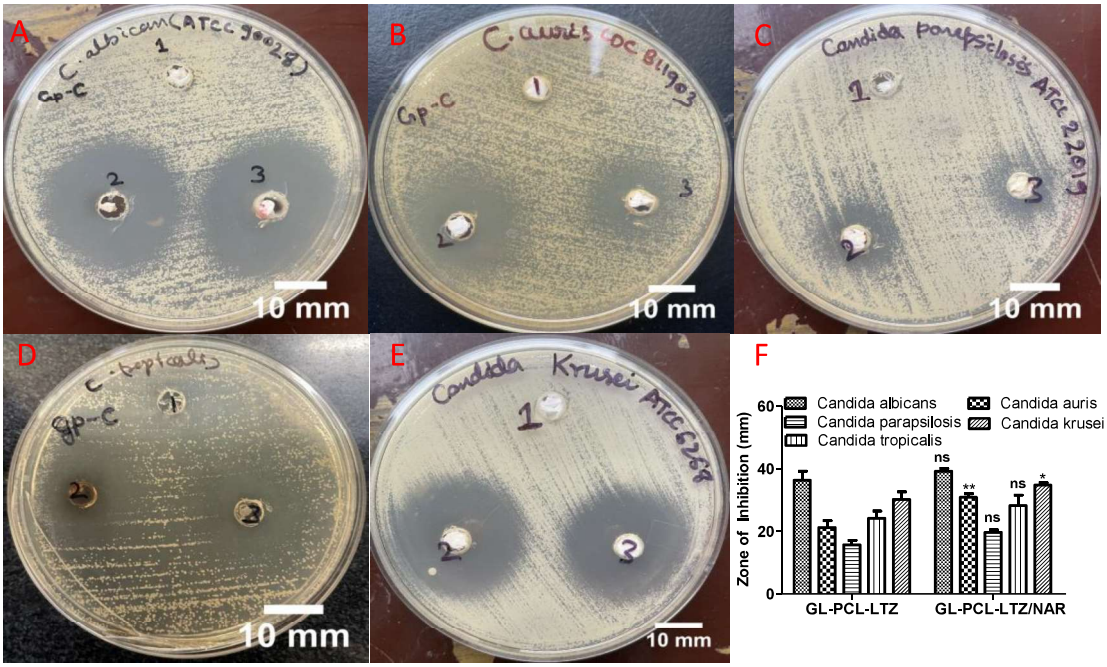

Figure 5.9 Antifungal activity of GL-PCL, GL-PCL-LTZ, GL-PCL-LTZ/NAR against (A) *C.albicans*; (B) *C.auri*; (C) *C.parapsilosis*; (D) *C.tropicalis*; (E) *C.krusei*; and (F) Zone of inhibition bar graph GL-PCL-LTZ and GL-PCL-LTZ/NAR (vertical bars in graph represent standard deviations (n=3))..

The antibiofilm study (MTT assay and SEM analysis) results *revealed that* GL-PCL-LTZ/NAR and GL-PCL-LTZ provides statistically significant (p-value < 0.001) biofilm inhibition (Figure 5.10B) of C.*albicans and C.tropicalis.* These results were further

supported by SEM images, proving efficacy of GL-PCL-LTZ/NAR nanofiber in inhibiting growth C.*albicans and C.tropicalis (Figure 5.10 A)*.

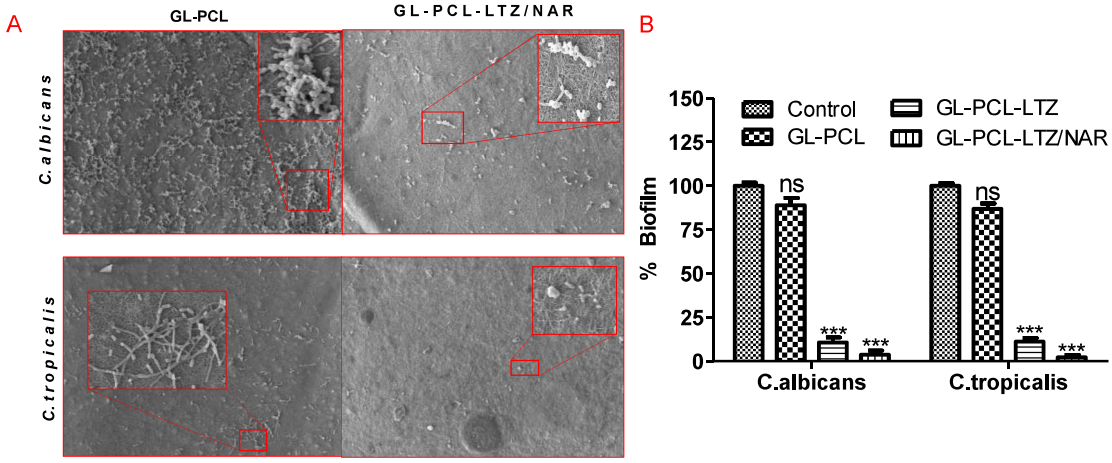

Figure 5.10 (A) SEM image of GL-PCL, GL-PCL-LTZ/NAR showing activity against *C.albicans* and *C.tropicalis* at 500X; (B) Antibiofilm activity (MTT assay) of GL-PCL, GL-PCL-LTZ & GL-PCL-LTZ/NAR against *C.albicans* and *C.tropicalis* (Vertical bars in graph represent standard deviations (n=3), 'ns' represent non significant and *** represent p value < 0.001)..

5.4.10 Hemocompatibility study

The hemocompatibility study of the GL-PCL, GL-PCL-LTZ, GL-PCL-NAR and GL-PCL-LTZ/NAR nanofiber demonstrated the haemolysis of 2.4±1.1%, 3.2±1.8%, 2.9±0.6% and 3.5±1.2%, respectively. The positive control and negative group showed the haemolysis 100% and 0.9±0.2%, respectively. This significant (p value <0.001) lower haemolysis rate of nanofiber proves that nanofiber are highly compatible with blood components and suitable for healing.

5.4.11 *In-vitro* cytocompatibility study

The *in-vitro* cytocompatibility study of the nanofiber showed that the nanofiber provides good cellular proliferation at 24, 48, and 72 hr, which is likely due to the 3D matrix structure of the nanofibers providing a suitable environment for cell adhesion and growth. Additionally, the nanofibers enhanced the cell proliferation (Figure 5.11) and migration, indicating their potential for wound-healing applications. The findings suggested that the

nanofibers treatment positively impacted the cellular behaviour and could be utilized as regenerative medicine to promote tissue regeneration [70].

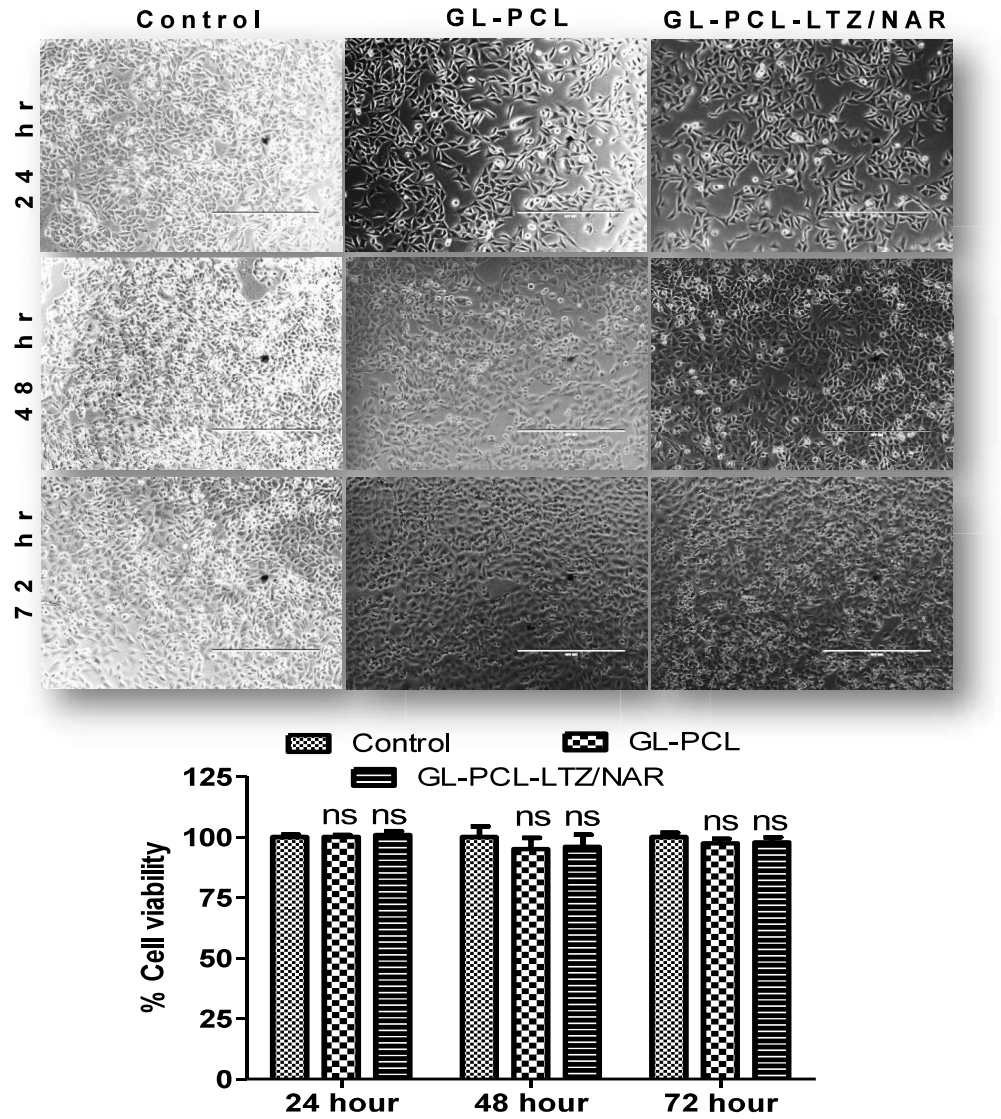

Figure 5.11 Phase contrast microscope image (Up) of HaCaT cytocompatibility study for GL-PCL and GL-PCL-LTZ/NAR nanofiber in 24, 48 and 72 hr (white scale bar = 400µm); Bar graph (down) representing % Cell viability of different nanofiber groups showing non-significant difference (p value>0.05) between Control and GL-PCL-LTZ/NAR & GL-PCL nanofiber (Vertical bars in graph represent standard deviations (n=3) and 'ns' represent non significant).

Additionally, the MTT assay data supported the microscopy results. The MTT data report for GL-PCL and GL-PCL-LTZ/NAR nanofibers showed a non-significant difference between the control and respective groups at 24, 48, and 72 hr (Figure 5.11), which

demonstrated good compatibility of prepared nanofibers with the HaCaT cell line and their role in promoting wound healing.

5.4.12 *In vivo* wound healing study

The *in vivo* wound closure results of different treatment groups are shown in Figure 5.12. All groups displayed signs of fungal infection on the fourth day, as shown in Figure 5.12A. After treatment on Day 12 of the study, the gauze-treated groups showed severe infection signs and the slowest wound healing compared to all groups. Specifically, the gauze-treated group had a wound area of 82.40±8.34% on Day 12 and 48.03±5.24% on Day 21, indicating the poorest wound closure. The GL-PCL group demonstrated a wound area of 63.88±2.99% on Day 12 and 35.04±3.07% on Day 21. This suggested improved wound healing observed in the GL-PCL group attributed to the nanofiber's role in preventing microbial invasion and providing optimal conditions for wound healing. Furthermore, the inclusion of NAR in GL-PCL-NAR nanofiber enhanced the wound healing efficacy of the nanofiber, resulting in a drop of 48.07±4.36% in wound area on the day 12 and a reduction of 18.50±1.26% in wound area on the day 21. A similar trend was observed in the GL-PCL-LTZ nanofiber, with a wound area of 40.76±2.44% on the 12th day and 15.57±3.21% on the 21st day. The concurrent administration of NAR and LTZ yielded remarkable outcomes, as shown by a wound closure rate of 29.75±3.75% on the 12th day and nearly imperceptible scarring by the 21st day. The observed outcome could be attributed to the antifungal and antioxidant properties exhibited by Luliconazole and naringenin in diabetic wound healing [207,300]. Furthermore, the GL-PCL-LTZ/NAR group showed a statistically significant (p-value < 0.001) wound closure compared to the untreated group on the 12th and 21st days. Additionally, GL-PCL nanofiber demonstrated a p-value < 0.01 on the 12th day and p-value < 0.01 on the 21st day.

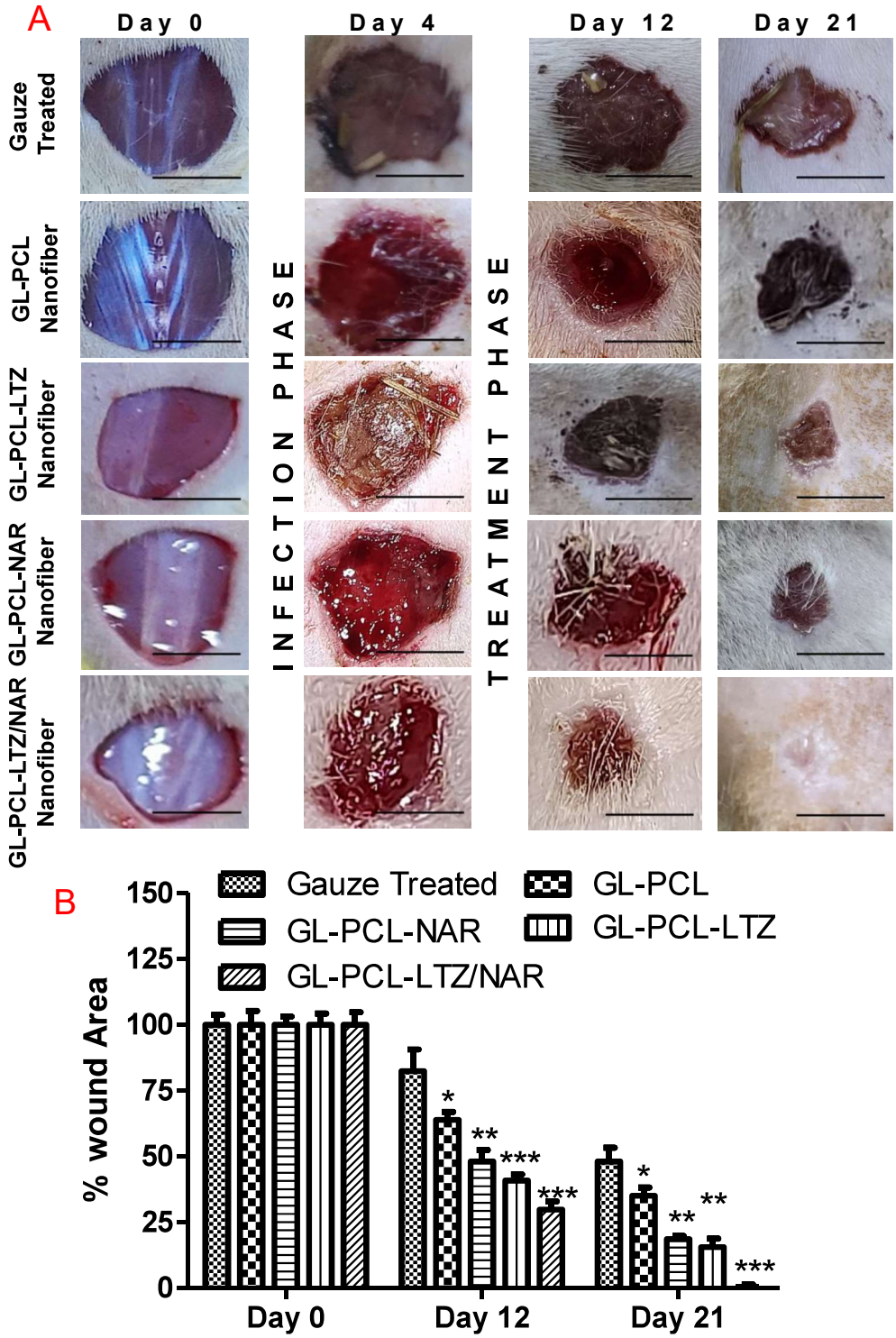

Figure 5.12 (A) Wound Closure study images of Gauze treated, GL-PCL nanofiber, and GL-PCL-NAR, GL-PCL-LTZ, and GL-PCL-LTZ/NAR group; (B) Quantitative data indicating % wound area of different treatment groups (Vertical bars in graph represent standard deviations (n=3), * represent p value < 0.05, ** represent p value < 0.01 and *** represent p value < 0.001).

5.4.13 Histopathological Study

The histopathological images of the Gauze-treated, GL-PCL, GL-PCL-NAR, GL-PCL-LTZ, and GL-PCL-LTZ/NAR nanofiber groups for days 12 and 21 are shown in Figure 5.13. The GL-PCL-NAR, GL-PCL-LTZ, and GL-PCL-LTZ/NAR nanofiber groups does not showed signs of any infection, However GL-PCL and gauze-treated group had severe to moderate signs of infection.

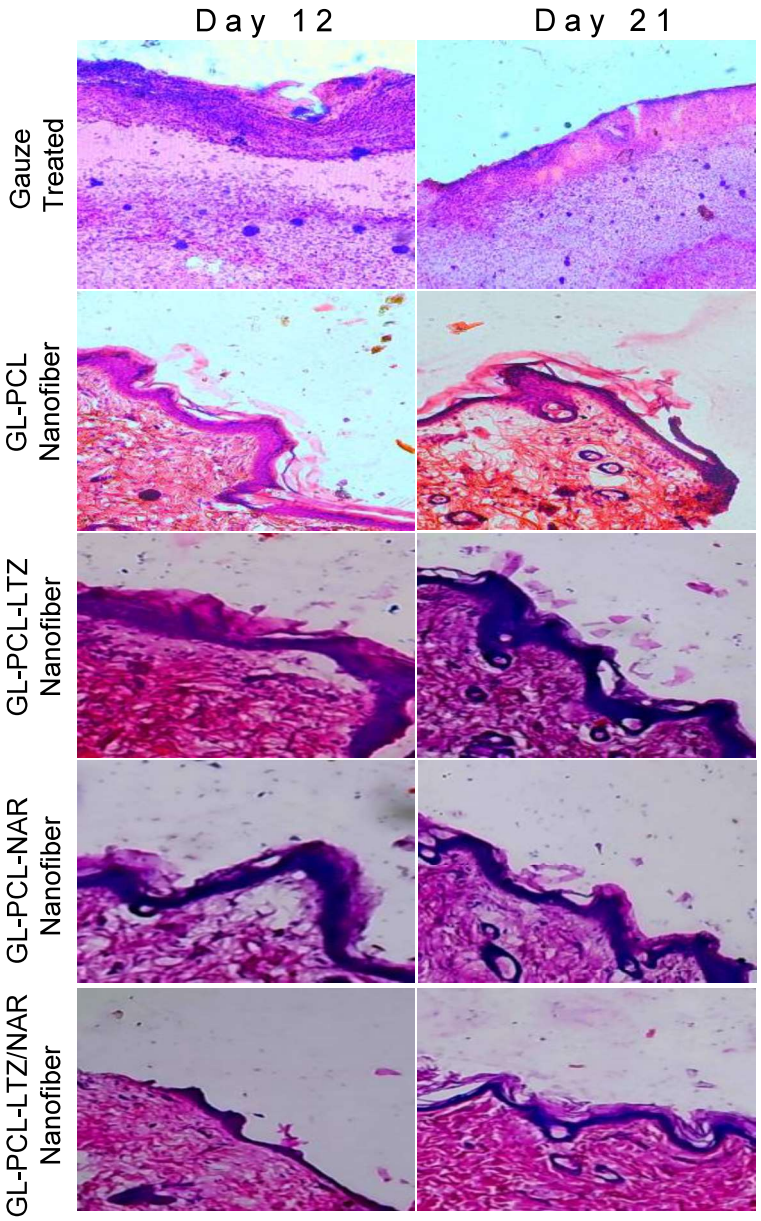

Figure 5.13 Histological H&E stained image of Gauze treated, GL-PCL, GL-PCL-NAR and GL-PCL-LTZ & GL-PCL-LTZ/NAR on day 12 and 21 of study

The GL-PCL showed infection signs only on day 12 compared to the gauze-treated group, which showed infection signs on the 12th and 21st days. This might be due to the ability of nanofibers to prevent microbial invasion, which helps the body counter infection. The GL-PCL-LTZ and GL-PCL-NAR showed no sign of infection and moderate reepithelization and granulation on day 12 and 21, respectively. The gauze-treated group showed minimal reepithelialisation, while the group treated with GL-PCL-LTZ/NAR demonstrated the highest reepithelialisation response compared to the other groups. Similarly, on the 12th day, it was observed that the GL-PCL-LTZ/NAR group exhibited a significantly higher level of neoangiogenesis compared to the blank and gauze-treated groups.

5.4.14 Laser Doppler study

The blood flow across wound sites in different groups, including gauze-treated, GL-PCL, GL-PCL-NAR, GL-PCL-LTZ, and GL-PCL-LTZ/NAR nanofiber groups, are shown in Figure 5.14 A. The GL-PCL nanofiber treatment group showed a statistically significant increase in blood flow around the wound area compared to the gauze treatment group, with a p-value of less than 0.05 on the 12th day and p value less than 0.01 on the 21st day. A similar pattern was observed between the GL-PCL and GL-PCL-NAR groups. The GL-PCL-NAR exhibited a higher blood flow across the wound on day 12th and 21st, with a statistically significant p-value of less than 0.01 (Figure 5.14 B). The GL-PCL-LTZ group not exhibited any statistically significant differences in blood flow improvement compared to the GL-PCL group. The GL-PCL-LTZ/NAR group showed the highest blood flow compared to all other groups, with a statistically significant p-value of less than 0.05 at the wound site. This observation might be attributed to an infection-free environment surrounding the wound and naringenin's antioxidant and anti-inflammatory properties.

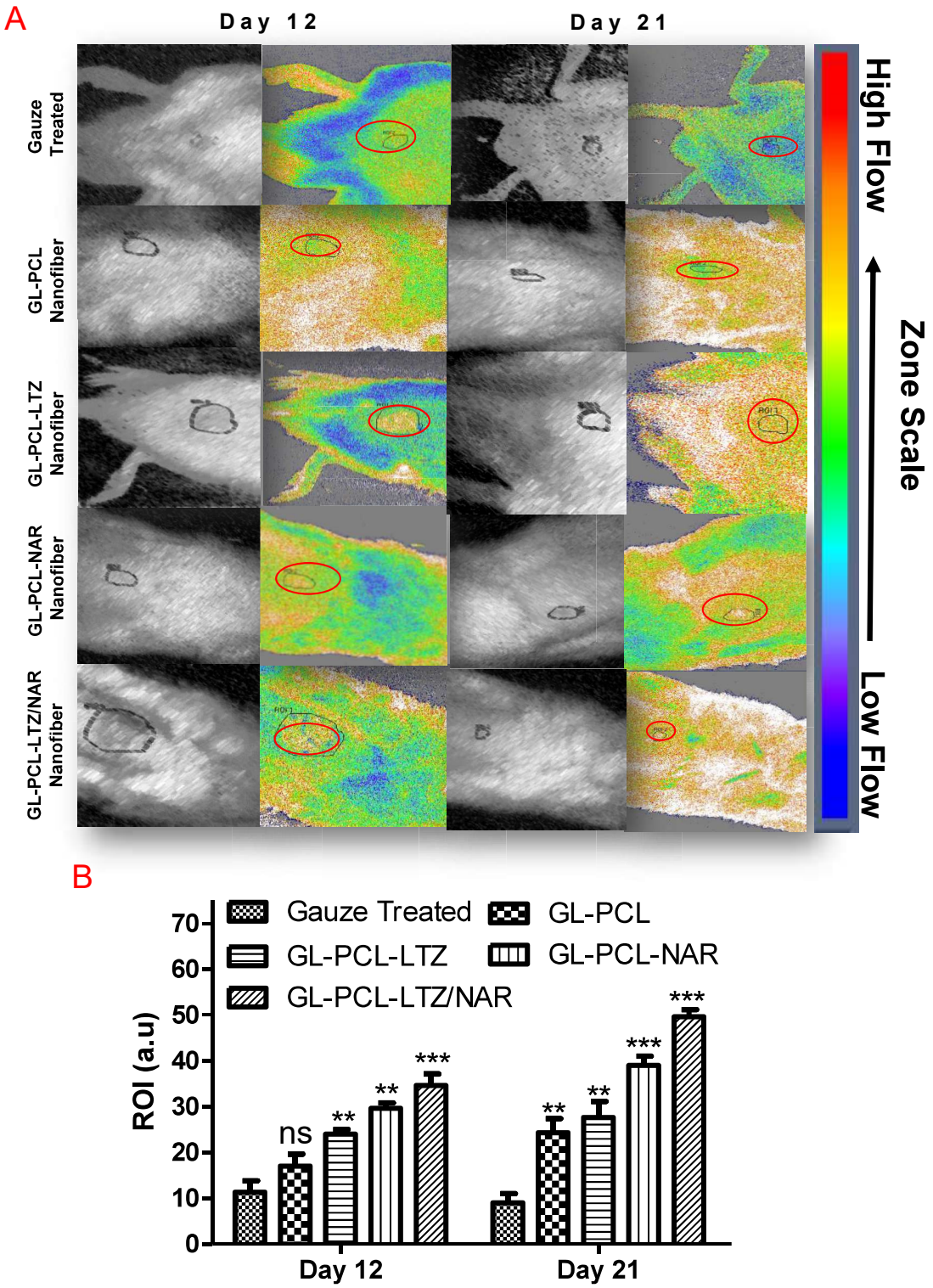

Figure 5.14 (A) Laser Doppler images (B) Graphical representation of the quantitative values obtain from laser doppler study (Vertical bars in graph represent standard deviations (n=3), 'ns' represent non significant, * represent p value < 0.05, ** represent p value < 0.01 and *** represent p value < 0.001).

5.5 Discussion & conclusions

Spectroscopy and microscopy of GL-PCL nanofibers confirmed uniform coating of gelatin over the surface of the PCL nanofiber, and a smooth surface with no visible defects or irregularities. The gelatin coating can provide favourable surface microenvironment for cell growth and differentiation. Also, the tripeptide site of gelatin acts as a binding site for integrins, which are essential for cell adhesion [301]. Furthermore, prepared nanofibers with interconnected nanostructure can improve cell proliferation, provides better nutrient and oxygen exchange, and ultimately leading to higher cell viability [302]. Additionally, the increased surface area of the nanofibers offers ample space for cell adhesion and migration, further enhancing tissue formation [303]. The nanofibers diameter for GL-PCL & GL-PCL-LTZ/NAR nanofiber was 213.35±52.55 nm and 379.67±166.62 nm, respectively. The increase in diameter for GL-PCL-LTZ/NAR nanofiber could be due to drug loading into nanofiber matrix that resulted in a thicker nanofiber structure.

Further, the contact angle study supports the findings of the SEM and TEM analysis, in which the PCL nanofiber showed a contact angle of 84.5°. In contrast, the coating of the gelatin over the nanofiber PCL nanofiber surface further reduces the contact angle of the nanofiber to 26.6◦. The reduced contact angle indicates that the GL coating promotes better wetting and adhesion, which can improve the interaction between the nanofiber matrix and biological fluids. These findings align with the literature, which indicates that the coating of the hydrophilic polymer over the surface of PCL nanofiber increases hydrophilicity and reduces the contact angle [304]. Additionally, the surface pH study proves that all nanofiber formulations are safe to apply over wounds. A very high or low pH could create irritation and discomfort for the patient, but the results showed that the pH of the GL-PCL nanofiber matrix was within the acceptable range for wound healing [305]. The FTIR characterization of the PCL, gelatin, naringenin, and nanofiber formulations shows us that the prepared

nanofibers are chemically compatible with each other, which ensures that the nanofibers will not undergo chemical reactions or degradation that could compromise their effectiveness in promoting wound healing [306]. Further, the XRD data show that both drugs are disturbed uniformly in the final formulation. This uniform distribution ensures that the drugs will be released consistently and efficiently, maximizing their therapeutic potential [307]. The XRD results also suggest that the nanofiber matrix maintains its structural integrity even after drug incorporation, further validating its suitability for diabetic wound healing. The DSC study demonstrates the thermal behaviour of luliconazole, naringenin, polycaprolactone, gelatin, and nanofibers. The data show the nanofiber matrix's melting point and degradation curve. This data is important in understanding the material behaviour of luliconazole, naringenin, polycaprolactone, gelatin, and nanofibers under fluctuating temperature variations. The entrapment efficiency of all nanofibers found to be greater than 75% indicates that the nanofibers have a strong ability to retain and deliver therapeutic agents to the wound site effectively. Additionally, the nanofiber's content uniformity results show a standard deviation value of <5% within two areas, which suggests that the drug within the nanofiber is uniformly distributed in the nanofiber matrix. This uniform drug distribution within the nanofiber matrix ensures consistent and reliable drug release [307]. The dissolution data modeling indicated that GL-PCL-LTZ/NAR nanofiber follows the release kinetic of the Peppas and Sahlin model, indicating a diffusion-controlled drug release mechanism. This suggests that the drug is slowly released from the nanofiber matrix over a prolonged period. This release pattern might be due to the swelling and erosion control diffusion of the drug through the nanofiber matrix of GL-PCL-LTZ/NAR, which is further proved by the n value of <0.45 as observed in the Korsemeyer-Peppas model, indicating non-Fickian release behaviour [308]. The controlled release of drugs from nanofibers is highly desirable in wound healing as it allows

for controlled delivery, minimizing side effects and maximizing therapeutic efficacy. Furthermore, the nanofiber's ability to release multiple drugs simultaneously opens up possibilities for combination therapy and other wound-healing applications. Additionally, the *in-vivo* bioimaging supports the *in-vitro* release study, showing a similar trend of release of the DiD dye from nanofibers in an *in-vivo* environment, providing valuable insights into drug delivery dynamics. The antifungal studies of the GL-PCL-LTZ and GL-PCL-LTZ/NAR fibers exhibited that the nanofibers were highly efficient at eradicating the growth of different *Candida* species. Further antibiofilm supports this observation, indicating that the GL-PCL-LTZ and GL-PCL-LTZ/NAR had significantly eradicated *C. albicans* and *C.tropicalis* in MTT assays, colony forming assay and scanning electron microscopy images. The *in-vitro* cytocompatibility study proves that all nanofibers effectively promote cellular proliferation due to the 3D morphological structure of the nanofiber matrix. Finally, the *In-vivo* wound closure study clearly indicated that GL-PCL-LTZ/NAR significantly improves the wound-healing potential of GL-PCL nanofiber. This might be due to the ability of the GL-PCL-LTZ/NAR to maintain an infection-free environment and enhance the blood flow around the wound area [197,309].

Finally, we could conclude that the GL-PCL-LTZ/NAR nanofiber has the potential to be a promising material for wound healing applications. Its ability to promote cellular proliferation and improve wound closure suggests that it could be used as a scaffold for wound healing dressing for chronic wounds.